IEEE Access
Multidisciplinary ⋮ Rapid Review ⋮ Open Access Journal

Received January 9, 2019, accepted March 1, 2019, date of current version April 3, 2019.

Digital Object Identifier 10.1109/ACCESS.2019.2904545

Multi-Sensor Space Debris Tracking for Space Situational Awareness With Labeled Random Finite Sets

BAISHEN WEI[1] AND BRETT D. NENER[2]
[1]School of Mechanical and Electric Engineering, Guangzhou University, Guangzhou 51006, China
[2]School of Electrical, Electronic, and Computer Engineering, The University of Western Australia, Perth, WA 6009, Australia

Corresponding author: Baishen Wei (baishen@gzhu.edu.cn)

ABSTRACT As a result of the dependence worldwide on satellite technology, it is now necessary to use advanced multi-target tracking algorithms for space debris tracking systems to maintain custody of space objects around the earth. One principal challenge is the correct association of observations with objects. This paper presents a multi-sensor, space-debris tracking algorithm using δ-generalized labeled multi-Bernoulli (δ-GLMB) filtering. The algorithm provides a solution to the key challenges (e.g., *detection uncertainty*, *data association uncertainty*, and *clutter*) in multiple object tracking. An efficient implementation of the multi-sensor δ-GLMB filter is proposed. In order to avoid exhaustively computing all the terms, we propose to use the ranked assignment algorithm with an extended assignment matrix for multiple sensors to determine the most significant terms. A measurement-based birth model is used to identify the previously unknown space objects. Sensors can have the same or different observation volumes. The expectation–maximization (EM) algorithm is used to approximate densities across observation volumes. The performance is demonstrated using the simulation results.

INDEX TERMS Space debris, δ-GLMB, multi-sensor, space situational awareness.

I. INTRODUCTION

The concept of space situational awareness (SSA) typically refers to three segments of knowledge: Near-Earth objects detection, space weather, and space surveillance and tracking of objects in Earth orbit [1], [2]. The near-Earth environment is populated with orbital debris after more than 50 years of space activity [3]. Accidental collisions may degrade the performance of a spacecraft or even cause fragmentation [4]. The rapid increase in the amount of space debris signals the potential for the collision cascade effect, commonly known as the ''Kessler Syndrome.'' Research shows that there is a need to focus on the debris detection for satellite safety and satellite collision avoidance [5]–[7]. Possible approaches to improve capabilities include: improving current system exploitation to discern small objects, upgrading tracking and sensor management algorithms to extend continuous monitoring, and building more sensor networks for increased spatial/temporal detection [5]. A multi-sensor space debris tracking approach is proposed in this paper to improve the tracking performance.

Multi-object tracking involves the estimation of the trajectories and the number of targets from noised measurements. False alarms, misdetections and data association uncertainty are the main challenges in multi-object tracking systems. The random finite set (RFS) [8], [9] is a popular multi-target estimation paradigm with applications in cell biology [10]–[12], traffic monitoring [13]–[16], field robotics [17]–[19], computer vision [11], [20]–[22], sonar [23], sensor network and distributed estimation [24]–[29], simultaneous localization and mapping [30]–[33], etc.

The multi-object state is modeled as a RFS. Because of the complexity of the Bayes filter, the Probability Hypothesis Density (PHD) [34], [35], Cardinalized PHD (CPHD) [36], [37] and multi-Bernoulli filters [38], [39] have been developed as approximations. An analytic solution, the δ-Generalized Labeled Multi-Bernoulli (δ-GLMB) filter and its efficient implementation were proposed in [40] and [41], respectively. Another efficient implementation with joint prediction and update and Gibbs sampling is detailed in [42]. Marginalized δ-GLMB (Mδ-GLMB) filter and Labeled Multi-Bernoulli (LMB) filter were proposed in [43] and [44], respectively, as two efficient approximations.

Finite Set Statistics (FISST)-based methods have been applied to the space debris problem in [6] and [45]–[55]. Reference [45] presents the application of several variations

The associate editor coordinating the review of this manuscript and approving it for publication was Yang Li.

of the RFS-based joint target detection and tracking filter for processing radar measurements. [47] presented a space object tracking approach with CPHD filtering and a measurement-based birth model. A labeled multi-Bernoulli filter for space object tracking was proposed in [6]. Reference [56] used GM-CPHD filtering and the consensus algorithm to achieve global space object tracking. Reference [57] presented a consensus LMB filtering for distributed space debris tracking. References [56] and [57] both presented a distributed space debris tracking approach. A recently published paper achieves distributed space debris tracking with a consensus algorithm and marginalized δ-GLMB filtering [58]. The distributed tracking system is scalable and robust. However, the tracking accuracy is worse than the centralized tracking system.

Multiple-node networks are widely used in tracking systems. Many algorithms have been proposed for multi-sensor fusion in the last thirty years [2], [26], [27], [59]–[65]. Multiple sensors can be used to reduce uncertainty about the object states and existence. The advantages of distributed and hierarchical systems include that they are scalable with respect to the network size and the bandwidth requirements are less than a centralized system. In a network that has no requirement for scalability and has large bandwidth and computation power, the centralized system is the best choice because it has the most accurate estimation. Centralized processing of measurements is currently employed as part of the U.S. Air Force Joint Space Operation Center (JSpOC). It is planned that the future system currently under development, i.e. the JSpOC Mission System (JMS) will also employ centralized data fusion [66].

However, in this paper we offer an alternative approach that will grow with the scale of the problem. Furthermore, most fusion algorithms assume that the sensors have the same observation volume and that targets do not go outside of this observation volume. However, this is not the case for space debris tracking. The relative positions between space debris and the Earth are not fixed except for those on geostationary equatorial orbit (GEO).

Preliminary results of centralized labeled RFS filtering was proposed in [67]. The method of [67] can only perform target tracking when the targets are inside of the observation volume. Therefore the information fusion can only be carried out for sensors with the same observation volume. Furthermore, the algorithm was only tested for targets assumed to follow a constant velocity dynamic model. This paper presents a multi-sensor space debris tracking algorithm with δ-GLMB filtering. An extended association map is created with measurements from every sensor in the update for multi-sensor δ-GLMB. The ranked assignment algorithm is used to truncate the multi-target densities. The measurement-based birth-model is used to capture previously unknown targets. The probability of detection outside the observation volume is set to zero; the estimation is essentially the prediction since the measurements are not available outside the observation volume. The Expectation Maximization (EM) algorithm is used to approximate densities across the observation volumes. With these modifications, the data fusion can be performed for sensors with different observation volumes as well as sensors with same observation volume.

The paper is organized as follows. Background on labeled RFS and the δ-GLMB filter is described in section II. The space debris dynamic model and Bayesian prediction method are provided in section III. Section IV details the multi-sensor δ-GLMB filtering. Numerical results are presented in Section V showing comparisons between a single sensor and multiple sensors with similar or complementary observation volumes. Concluding remarks are given in Section VI.

II. BACKGROUND

This section describes the multi-target tracking formulation of labeled RFS and the propagation of δ-GLMB filtering. Subsection II-A summarizes labeled RFS and Bayesian multi-target filtering, followed by the measurement likelihood function and the transition kernel in subsection II-B and II-C. The δ-GLMB recursion is described in subsection II-D.

In this paper, we use

$$\delta_Y(X) \triangleq \begin{cases} 1, & \text{if } X = Y \\ 0, & \text{otherwise.} \end{cases} \tag{1}$$

The inclusion function is

$$1_Y(X) \triangleq \begin{cases} 1, & \text{if } X \subseteq Y \\ 0, & \text{otherwise.} \end{cases} \tag{2}$$

The inner product is $\langle f, g \rangle \triangleq \int f(x)g(x)dx$ and the exponential is $h^X \triangleq \Pi_{x \in X} h(x)$.

For the rest of this paper, lowercase letters (e.g. $x, \mathbf{x}$) are used to represent single-object states, while uppercase letters (e.g. $X, \mathbf{X}$) are used to represent multi-object states. Bolded symbols (e.g. $\mathbf{x}, \mathbf{X}, \boldsymbol{\pi}$) are used to distinguish labeled states and their distributions from unlabeled ones. Blackboard bold (e.g. $\mathbb{X}, \mathbb{N}$) is used to represent spaces.

A. LABELED RFS AND BAYESIAN MULTI-TARGET FILTERING

An RFS is a finite-set-valued random variable. Every dynamic state $x \in \mathbb{X}$ has a unique label $\ell \in \mathbb{L} = \{\alpha_i : i \in \mathbb{N}\}$. Let the projection $\mathcal{L}((x, \ell)) = \ell$ be denoted by $\mathcal{L} : \mathbb{X} \times \mathbb{L} \to \mathbb{L}$, then the function $\Delta(\mathbf{X}) \triangleq \delta_{|\mathbf{X}|}(|\mathcal{L}(\mathbf{X})|)$ is called the *distinct label indicator* which means that $\mathbf{X}$ has the same cardinality as its labels $\mathcal{L}(\mathbf{X}) = \{\mathcal{L}(\mathbf{x}) : \mathbf{x} \in \mathbf{X}\}$ [40], [41].

Assume that there are $N(k)$ targets at time k with states $\boldsymbol{x}_{k,1}, \ldots, \boldsymbol{x}_{k,N(k)}$ and state space $\mathbb{X} \times \mathbb{L}$, and $M(k)$ measurements $z_{k,1}, \ldots, z_{k,M(k)}$ with observation space $\mathbb{Z}$. Then the *multi-target state* and *multi-target observation* is

$$\mathbf{X}_k = \{\boldsymbol{x}_{k,1}, \ldots, \boldsymbol{x}_{k,N(k)}\} \tag{3}$$

$$Z_k = \{z_{k,1}, \ldots, z_{k,M(k)}\} \tag{4}$$

Let $\boldsymbol{\pi}_k(\cdot|Z_k)$ denote the *multi-target filtering density* and $\boldsymbol{\pi}_{k+1|k}$ denote the *multi-target prediction density*. Then the target density is propagated according to

$$\boldsymbol{\pi}_k(\mathbf{X}_k|Z_k) = \frac{g_k(Z_k|\mathbf{X}_k)\boldsymbol{\pi}_{k|k-1}(\mathbf{X}_k)}{\int g_k(Z_k|\mathbf{X}_k)\boldsymbol{\pi}_{k|k-1}(\mathbf{X}_k)\delta\mathbf{X}} \tag{5}$$

$$\boldsymbol{\pi}_{k+1|k}(\mathbf{X}_{k+1}) = \int \mathbf{f}_{k+1|k}(\mathbf{X}_{k+1}|\mathbf{X}_k)\boldsymbol{\pi}_k(\mathbf{X}_k|Z_k)\,\delta\mathbf{X}_k \tag{6}$$

where $\mathbf{f}_{k+1|k}(\cdot|\cdot)$ is the *multi-target transition density* to time $k+1$, $g_k(\cdot|\cdot)$ is the *multi-target likelihood function* at time k. The underlying models of target births, deaths and motions are encapsulated in the multi-target transition density while the underlying models for detections and false alarms are encapsulated in the multi-target likelihood function.

For convenience, we denote $g \triangleq g_k$, $\mathbf{f} \triangleq \mathbf{f}_{k+1|k}$, $\boldsymbol{\pi}_+ \triangleq \boldsymbol{\pi}_{k+1|k}$, $\boldsymbol{\pi} \triangleq \boldsymbol{\pi}_k$, $\mathbb{B} \triangleq \mathbb{L}_{k+1}$, $\mathbb{L}_+ \triangleq \mathbb{L} \cup \mathbb{B}$.

B. MEASUREMENT LIKELIHOOD FUNCTION

Each state $(x, \ell) \in \mathbf{X}$ has the probability $p_D(x, \ell)$ to be detected and generates a measurement with likelihood function $g(z|x, \ell)$, and has a probability $1 - p_D(x, \ell)$ to be miss-detected. The measurement set Z is a superposition of detected objects and Poisson clutter with intensity function κ.

An association map is denoted by $\theta: \mathbb{L} \to \{0, 1, \ldots, |Z|\}$ such that $\theta(i) = \theta(i') > 0$ implies $i = i'$. The set Θ of all such association maps is used to denote the association space. The subset of association maps with domain I is denoted by $\Theta(I)$.

The multi-object likelihood is given by [40], [41]

$$g(Z|\mathbf{X}) = e^{-<\kappa,1>}\kappa^Z \sum_{\theta\in\Theta(\mathcal{L}(\mathbf{X}))} [\psi_Z(\cdot;\theta)]^{\mathbf{X}}. \tag{7}$$

where

$$\psi_Z(x, \ell; \theta) = \begin{cases} \dfrac{p_D(x, \ell)g(z_{\theta(\ell)}|x, \ell)}{\kappa(z_{\theta(\ell)})}, & \text{if } \theta(\ell) > 0 \\ 1 - p_D(x, \ell), & \text{if } \theta(\ell) = 0 \end{cases} \tag{8}$$

C. MULTI-TARGET TRANSITION KERNEL

Each state $(x, \ell) \in \mathbf{X}$ has the probability $p_S(x, \ell)$ to survive and evolve to the next step with new state (x_+, ℓ_+), or has the probability of $1 - p_S(x, \ell)$ to die. The birth density is

$$\mathbf{f}_B(\mathbf{Y}) = \Delta(\mathbf{Y})\omega_B(\mathcal{L}(\mathbf{Y}))[p_B]^{\mathbf{Y}} \tag{9}$$

where p_B and ω_B are given parameters of the birth density.

The multi-target state at the next time step $\mathbf{X}_+$ includes two parts: the new born targets and the surviving targets. The multi-target transition density is [40], [41]

$$\mathbf{f}(\mathbf{X}_+|\mathbf{X}) = \mathbf{f}_S(\mathbf{X}_+ \cap (\mathbb{X} \times \mathbb{L})|\mathbf{X})\mathbf{f}_B(\mathbf{X}_+ - (\mathbb{X} \times \mathbb{L})) \tag{10}$$

where

$$\mathbf{f}_S(\mathbf{W}|\mathbf{X}) = \Delta(\mathbf{W})\Delta(\mathbf{X})1_{\mathcal{L}(\mathbf{X})}(\mathcal{L}(\mathbf{W}))[\Phi(\mathbf{W};\cdot)]^{\mathbf{X}} \tag{11}$$

$$\Phi(\mathbf{W}; x, \ell) = \begin{cases} p_S(x, \ell)f(x_+|x, \ell), & \text{if } (x_+, \ell) \in \mathbf{W} \\ 1 - p_S(x, \ell), & \text{if } \ell \notin \mathcal{L}(\mathbf{W}) \end{cases} \tag{12}$$

D. DELTA-GENERALIZED LABELED MULTI-BERNOULLI

The δ-GLMB filter has the form of

$$\boldsymbol{\pi}(\mathbf{X}) = \Delta(\mathbf{X}) \sum_{(I,\xi)\in\mathcal{F}(\mathbb{L})\times\Xi} \omega^{(I,\xi)}\delta_I(\mathcal{L}(\mathbf{X}))[p^{(\xi)}]^{\mathbf{X}}. \tag{13}$$

Here each I represents a set of track labels and each ξ represents a history of association maps, Ξ is a discrete space. The pair $(I, \xi) \in \mathcal{F}(\mathbb{L}) \times \Xi$ is a *hypothesis*. The associated weight means the existence probability of the hypothesis. $p^{(\xi)}$ is the density of the kinematic state.

Assume that the multi-target prediction density for the current time is a δ-GLMB of the form (13), then the multi-target posterior probability density is a δ-GLMB given by

$$\pi(\mathbf{X}|Z) = \Delta(\mathbf{X}) \sum_{(I,\xi)\in\mathcal{F}(\mathbb{L})\times\Xi} \sum_{\theta\in\Theta(I)} \omega^{(I,\xi,\theta)}(Z)\cdot\delta_I \times(\mathcal{L}(\mathbf{X}))[p^{(\xi,\theta)}(\cdot|Z)]^{\mathbf{X}} \tag{14}$$

where

$$\omega^{(I,\xi,\theta)}(Z) \propto \omega^{(I,\xi)}[\eta_Z^{(\xi,\theta)}]^I \tag{15}$$

$$\eta_Z^{(\xi,\theta)}(\ell) = \langle p^{(\xi)}(\cdot, \ell), \psi(\cdot, \ell; \theta)\rangle \tag{16}$$

$$p^{(\xi,\theta)}(x, \ell|Z) = \frac{p^{(\xi)}(x, \ell)\psi_Z(x, \ell; \theta)}{\eta_Z^{(\xi,\theta)}(\ell)} \tag{17}$$

Assume that the multi-target filtering density is a δ-GLMB of the form (13), then the multi-target prediction density is a δ-GLMB given by

$$\pi_+(\mathbf{X}_+) = \Delta(\mathbf{X}_+) \sum_{(I_+,\xi)\in\mathcal{F}(\mathbb{L}_+)\times\Xi} \omega_+^{(I_+,\xi)}\delta_{I_+}(\mathcal{L}(\mathbf{X}_+))\,[p_+^{(\xi)}]^{\mathbf{X}_+} \tag{18}$$

where

$$\omega_+^{(I_+,\xi)} = \omega_S^{(\xi)}(I_+ \cap \mathbb{L})\omega_B(I_+ \cap \mathbb{B}) \tag{19}$$

$$\omega_S^{(\xi)}(L) = [\eta_S^{(\xi)}]^L \sum_{I\supseteq L} [1 - \eta_S^{(\xi)}]^{I-L}\omega^{(I,\xi)} \tag{20}$$

$$p_S^{(\xi)}(x, \ell) = \frac{\langle p_S(\cdot, \ell)f(x|\cdot, \ell), p^{(\xi)}(\cdot, \ell)\rangle}{\eta_S^{(\xi)}(\ell)} \tag{21}$$

$$p_+^{(\xi)}(x, \ell) = 1_{\mathbb{L}}(\ell)p_S^{(\xi)}(x, \ell) + 1_{\mathbb{B}}(\ell)p_B(x, \ell) \tag{22}$$

$$\eta_S^{(\xi)}(\ell) = \langle p_S(\cdot, \ell), p^{(\xi)}(\cdot, \ell)\rangle \tag{23}$$

III. SPACE DEBRIS DYNAMIC MODEL AND BAYESIAN PREDICTION

It is very difficult to calculate the Markov transition density function of space objects because the space dynamic model is much more complicated than the constant velocity or the constant turn model. However, we can approximate the transition density function of space debris with the help of the software Turboprop [68] and the unscented transform [69]. Turboprop can be called as a function in MATLAB and has a package of functions to calculate the trajectories of space objects. The elements in Turboprop include the Earth Orientation and atmospheric drag model, the lunar gravity models LP100K, GLGM-2 and LP150Q, the Earth gravity models

JGM-3, GGM02C and WGS-84, JPL planetary ephemerides DE403 and DE405 and solar radiation pressure model.

The coordinate system used in this paper is an Earth-centered, Earth-fixed (ECEF) geographic and Cartesian coordinate system. The point (0, 0, 0) is defined as the center of mass of the Earth and the axes are aligned with the international reference pole and international reference meridian.

The Jet Propulsion Laboratory Development Ephemeris (JPL DE) are generally created to support spacecraft missions to the planets. JPL DE designates a series of models consisting of representations of accelerations, velocities and positions of major Solar System bodies.

The acceleration caused by the solar radiation pressure is [70]

$$\ddot{\mathbf{r}}_{SRP} = p_{SR} c_R \frac{A}{m} \frac{\mathbf{r}}{|\mathbf{r}|} \tag{24}$$

where p_{SR} is the pressure of solar radiation in Pa. c_R is the solar radiation coefficient and is taken as 1.5. m (0.05 kg in this paper) is the mass of the space debris. A (0.01 m^2 in this paper) is the cross-sectional area facing the Sun. $\mathbf{r}$ is the vector from the center of the Sun to the space debris. Solar radiation behaves like a flux of particles emitted by the sun [71]. Solar radiation is the dominant source of radiation pressure. Even though vector $\mathbf{r}$ is from the center of the Sun to the space debris, the coordination system used in this paper is ECEF system.

The mass concentration model is a gravity field where the total acceleration is determined by point masses. The total acceleration is

$$\ddot{\mathbf{r}}_{pointmass} = -G \sum_i \frac{m_i \bar{\mathbf{r}}_i}{r_i^3} \tag{25}$$

where $\bar{\mathbf{r}}_i$ is the vector from the point mass to the space debris, r_i is the magnitude of $\bar{\mathbf{r}}_i$ and m_i is the mass of i-th point, and $G = 6.67428 \times 10^{-20} km^3/(kg \cdot sec^2)$. This paper takes the Sun, the Earth, Venus, Jupiter and the Moon into consideration.

The gravity field is modeled using U, an aspherical potential function

$$U(x, y, z) = \frac{\mu}{r} \sum_{n=2}^{\infty} \sum_{m=0}^{n} (\frac{R}{r})^n \bar{A}_{n,m}[\frac{z}{r}]\{\bar{C}_{n,m}\bar{E}_m + \bar{S}_{n,m}\bar{F}_m\} \tag{26}$$

where

$$r = \sqrt{x^2 + y^2 + z^2} \tag{27}$$

$$\bar{E}_m = \bar{E}_1\bar{E}_{m-1} - \bar{F}_1\bar{F}_{m-1}, \quad \bar{E}_0, \bar{E}_1 = \frac{x}{r} \tag{28}$$

$$\bar{F}_m = \bar{F}_1\bar{E}_{m-1} - \bar{E}_1\bar{F}_{m-1}, \quad \bar{F}_0, \bar{F}_1 = \frac{y}{r} \tag{29}$$

R is the radius of the central body, μ is the gravitational parameter and n and m are the degree and order of the spherical harmonic model respectively. $\bar{C}_{n,m}$ and $\bar{S}_{n,m}$ are normalized coefficients for the magnitude of the spherical harmonics. $\bar{A}_{n,m}[\alpha = \frac{z}{r}]$ is a normalized, derived Legendre function.

The acceleration from atmospheric drag is computed with the equations

$$\begin{aligned} \ddot{x}_{drag} &= -\frac{C_D}{2}\frac{A}{m}\rho V_{a,x}|V_a| \\ \ddot{y}_{drag} &= -\frac{C_D}{2}\frac{A}{m}\rho V_{a,y}|V_a| \\ \ddot{z}_{drag} &= -\frac{C_D}{2}\frac{A}{m}\rho V_{a,z}|V_a| \end{aligned} \tag{30}$$

where C_D is the coefficient of drag and $\frac{A}{m}$ is the area-to-mass ratio of the space debris. $V_{a,x}$, $V_{a,y}$ and $V_{a,z}$ are the velocity components of the space debris with respect to the atmosphere and $|V_a|$ is the magnitude.

The unscented transform is used in the nonlinear projection of mean and covariance estimations. The unscented transform approximates the probability density function (PDF) by a set of sigma points. Assume that each single target density $p(x)$ is a Gaussian mixture of the form $\sum_{i=1}^{N} \omega_i \mathcal{N}(x; m_i, P_i)$ and the Gaussian item is n-dimensional, then the state of space debris is propagated as shown in Table 1.

TABLE 1. State propagation of space debris.

input:$\{\omega_i, m_i, P_i\}_{i=1}^{N}$ output:$\{\omega_i^+, m_i^+, P_i^+\}_{i=1}^{N}$
for i=1:N 1):$2n+1$ weighted sigma points $S^{(j)} = \{(W^{(j)}, \chi^{(j)})\}$ are chosen to represent the Gaussian. 2):every sigma point is propagated with the help of Turboprop. 3):the predicted Gaussian is reconstructed with the predicted sigma points. end

The sigma-points are chosen as follows:

$$\chi^{(0)} = m, \quad W^{(0)} = \frac{\kappa}{n+\kappa}, \quad j = 0$$

$$\chi^{(j)} = m + (\sqrt{(n+\kappa)P})_j, \quad W^{(j)} = \frac{1}{2(n+\kappa)}, \; j = 1, \ldots, n$$

$$\chi^{(j)} = m - (\sqrt{(n+\kappa)P})_j, \quad W^{(j)} = \frac{1}{2(n+\kappa)}, \; j = n+1, \ldots, 2n$$

where n represents the dimension of state vector which is 6 in this paper, $\sum_{j=0}^{2n} W^{(j)} = 1$, $\left(\sqrt{(n+\kappa)P}\right)_j$ is the jth row or column of square root of $\sqrt{(n+\kappa)P}$, κ is the scaling parameter which is 2 in this paper.

IV. MULTI-SENSOR δ-GLMB FILTERING

Subsection IV-A summarizes the multi-sensor measurement likelihood function. Subsection IV-B details the multi-sensor δ-GLMB update. The ranked assignment problem for multi-sensor δ-GLMB is presented in subsection IV-C. Subsection IV-D presents the computation of the multi-sensor δ-GLMB parameters. The EM algorithm for updating with non-uniform detection probability is presented in subsection IV-E. Subsection IV-F details the measurement-based

birth model. Subsection IV-G discusses the problem of synchronization and inconsistency.

A. MULTI-SENSOR MEASUREMENT LIKELIHOOD FUNCTION

For clarity of illustration, we only show the situation of two sensors, however, extension to cases with more sensors can be easily made.

Enumerating $Z_1 = \{z_{1,1}, \ldots, z_{1,|Z_1|}\}$, $Z_2 = \{z_{2,1}, \ldots, z_{2,|Z_2|}\}$, $I = \{\ell_1, \ldots, \ell_{|I|}\}$, then an association map for sensor j is a function θ_j: $\mathbb{L} \to \{0, 1, \ldots, |Z_j|\}$ such that $\theta_j(i) = \theta_j(i') > 0$ implies $i = i'$. An association map for two sensors is a function (θ_1, θ_2): $\mathbb{L} \to \{0, 1, \ldots, |Z_1|\} \times \{0, 1, \ldots, |Z_2|\}$ such that $(\theta_1, \theta_2)(i) = (\theta_1, \theta_2)(i')$ with $(\theta_1(i)|\theta_2(i)) > 0$ and $(\theta_1(i')|\theta_2(i')) > 0$ implies $i = i'$.

At time k, the multi-object likelihood is given by

$$\begin{aligned}
&g(Z_1, Z_2|\mathbf{X}) \\
&= g(Z_1|\mathbf{X})g(Z_2|\mathbf{X}) \\
&= e^{-\langle\kappa_1,1\rangle}\kappa_1^{Z_1}\sum\nolimits_{\theta_1\in\Theta_1(\mathcal{L}(\mathbf{X}))}[\psi_{Z_1}(\cdot;\theta_1)]^{\mathbf{X}} \\
&\quad\cdot e^{-\langle\kappa_2,1\rangle}\kappa_2^{Z_2}\sum\nolimits_{\theta_2\in\Theta_2(\mathcal{L}(\mathbf{X}))}[\psi_{Z_2}(\cdot;\theta_2)]^{\mathbf{X}} \\
&= e^{-\langle\kappa_1,1\rangle}\kappa_1 e^{-\langle\kappa_2,1\rangle}\kappa_2\sum_{\substack{\theta_1\in\Theta_1(\mathcal{L}(\mathbf{X})),\\ \theta_2\in\Theta_2(\mathcal{L}(\mathbf{X}))}}[\psi_{Z_1,Z_2}(\cdot;\theta_1,\theta_2)]^{\mathbf{X}} \\
&= e^{-\langle\kappa_1,1\rangle}\kappa_1 e^{-\langle\kappa_2,1\rangle}\kappa_2\sum_{(\theta_1,\theta_2)\in\Theta_{1,2}(\mathcal{L}(\mathbf{X}))}[\psi_{Z_1,Z_2}(\cdot;(\theta_1,\theta_2))]^{\mathbf{X}}
\end{aligned} \tag{31}$$

where

$$\begin{aligned}
&\psi_{Z_1,Z_2}(x,\ell;(\theta_1,\theta_2)) \\
&= \begin{cases}
\dfrac{p_{D_1}(x,\ell)g_1(z_{\theta_1(\ell)}|x,\ell)}{\kappa_1(z_{\theta_1(\ell)})}\cdot\dfrac{p_{D_2}(x,\ell)g_2(z_{\theta_2(\ell)}|x,\ell)}{\kappa_2(z_{\theta_2(\ell)})}, \\
\qquad\text{if } \begin{cases}\theta_1(\ell)>0,\\ \theta_2(\ell)>0\end{cases} \\
(1-p_{D_1}(x,\ell))\cdot\dfrac{p_{D_2}(x,\ell)g_2(z_{\theta_2(\ell)}|x,\ell)}{\kappa_2(z_{\theta_2(\ell)})}, \\
\qquad\text{if } \begin{cases}\theta_1(\ell)=0,\\ \theta_2(\ell)>0\end{cases} \\
\dfrac{p_{D_1}(x,\ell)g_1(z_{\theta_1(\ell)}|x,\ell)}{\kappa_1(z_{\theta_1(\ell)})}\cdot(1-p_{D_2}(x,\ell)), \\
\qquad\text{if } \begin{cases}\theta_1(\ell)>0,\\ \theta_2(\ell)=0\end{cases} \\
(1-p_{D_1}(x,\ell))\cdot(1-p_{D_2}(x,\ell)), \\
\qquad\text{if } \begin{cases}\theta_1(\ell)=0,\\ \theta_2(\ell)=0\end{cases}
\end{cases}
\end{aligned} \tag{32}$$

B. MULTI-SENSOR δ-GLMB FILTER UPDATE

Since the prediction for the multi-sensor δ-GLMB filter is the same as for a single sensor, we only present the update for multi-sensor δ-GLMB.

If the current multi-target prediction density is a δ-GLMB of the form (13), then the multi-sensor multi-target filtering density is a δ-GLMB given by

$$\begin{aligned}
&\pi(\mathbf{X}|Z_1,Z_2) \\
&\quad= \Delta(\mathbf{X})\sum_{(I,\xi)\in\mathcal{F}(\mathbb{L})\times\Xi}\sum_{(\theta_1,\theta_2)\in\Theta_{1,2}(I)}\omega^{(I,\xi,(\theta_1,\theta_2))}(Z_1,Z_2) \\
&\qquad\cdot\delta_I(\mathcal{L}(\mathbf{X}))[p^{(\xi,(\theta_1,\theta_2))}(\cdot|Z_1,Z_2)]^{\mathbf{X}}
\end{aligned} \tag{33}$$

where

$$\omega^{(I,\xi,(\theta_1,\theta_2))}(Z_1,Z_2) \propto \omega^{(I,\xi)}[\eta_{Z_1,Z_2}^{\xi,(\theta_1,\theta_2)}]^I, \tag{34}$$

$$p^{(\xi,(\theta_1,\theta_2))}(x,\ell|Z_1,Z_2) = \frac{p^{(\xi)}(x,\ell)\psi_{Z_1,Z_2}(x,\ell;(\theta_1,\theta_2))}{\eta_{Z_1,Z_2}^{(\xi,(\theta_1,\theta_2))}(\ell)} \tag{35}$$

$$\eta_{Z_1,Z_2}^{(\xi,(\theta_1,\theta_2))}(\ell) = \langle p^{(\xi)}(\cdot,\ell), \psi_{Z_1,Z_2}(\cdot,\ell;(\theta_1,\theta_2))\rangle \tag{36}$$

Equation (33) has a similar form as equation (14). The main difference lies in the measurement set, association map and measurement likelihood function. Instead of measurement set Z for single sensor, the measurement set for multi-sensor is (Z_1, Z_2). The association map for single sensor is θ. The association map for multi-sensor is (θ_1, θ_2). The measurement likelihood function for multi-sensor is presented in IV-A.

C. RANKED ASSIGNMENT PROBLEM FOR MULTI-SENSOR DELTA-GLMB UPDATE

Each hypothesis (I, ξ) with weight $\omega^{(I,\xi)}$ generates a new set of hypotheses $(I, (\xi, (\theta_1, \theta_2)))$, with corresponding weights $\omega^{(I,\xi,(\theta_1,\theta_2))}(Z_1, Z_2) \propto \omega^{(I,\xi)}[\eta_{Z_1,Z_2}^{\xi,(\theta_1,\theta_2)}]^I$. The most significant hypotheses can be chosen without exhaustively computing all the new components if the association maps can be generated in decreasing order of $\eta_{Z_1,Z_2}^{\xi,(\theta_1,\theta_2)}$. Ranked assignment can be used to solve this problem.

With the new definition of the association map for two sensors, let $(Z_1)\cup(Z_2)\cup(Z_1\times Z_2)$ denote the measurements from two sensors (Z_1, Z_2). (Z_1) denotes that only measurements from sensor1 are assigned to targets. (Z_2) denotes that only measurements from sensor2 are assigned to targets. $(Z_1 \times Z_2)$ denotes that measurements from sensor1 and sensor2 are all assigned to targets, i.e. $(Z_1 \times Z_2) \triangleq \{(z_1, z_2) : z_1 \in Z_1, z_2 \in Z_2\}$.

An $|I| \times |(Z_1, Z_2)|$ *assignment matrix* S can be used to represent each association map. S consists of 0 or 1 entries. Each column and row of S sums to either 0 or 1. For $i \in \{1, \ldots, |I|\}, j \in \{1, \ldots, |(Z_1, Z_2)|\}$, $S_{i,j} = 1$ means that only the jth measurement is assigned to track ℓ_i.

In an optimal assignment problem, the *cost matrix* is the $|I| \times |(Z_1, Z_2)|$ matrix $C_{Z_1,Z_2}^{(I,\xi)}$ with elements:

$$\begin{aligned}
&(C_{Z_1,Z_2}^{(I,\xi)})_{i,j} \\
&= -\ln\begin{cases}
\dfrac{\langle p^{(\xi)}(\cdot,\ell_i), p_{D_1}(\cdot,\ell_i)g_1(z_j|\cdot,\ell_i)(1-p_{D_2})(\cdot;\ell_i)\rangle}{\langle p^{(\xi)}(\cdot,\ell_i),(1-p_{D_1})(\cdot,\ell_i)(1-p_{D_2})(\cdot;\ell_i)\rangle\kappa_1(z_j)}, \\
\qquad\text{for } \{_{j\in\{1,\ldots,|Z_1|\}}^{i\in\{1,\ldots,|I|\}} \\
\dfrac{\langle p^{(\xi)}(\cdot,\ell_i),(1-p_{D_1})(\cdot;\ell_i)p_{D_2}(\cdot,\ell_i)g_2(z_j|\cdot,\ell_i)\rangle}{\langle p^{(\xi)}(\cdot,\ell_i),(1-p_{D_1})(\cdot;\ell_i)(1-p_{D_2})(\cdot,\ell_i)\rangle\kappa_2(z_j)}, \\
\qquad\text{for } \{_{j\in\{1,\ldots,|Z_2|\}}^{i\in\{1,\ldots,|I|\}} \\
\dfrac{\langle p^{(\xi)}(\cdot,\ell_i), p_{D_1}(\cdot,\ell_i)g_1(z_j|\cdot,\ell_i)p_{D_2}(\cdot,\ell_i)g_2(z_j|\cdot,\ell_i)\rangle}{\langle p^{(\xi)}(\cdot,\ell_i),(1-p_{D_1})(\cdot;\ell_i)(1-p_{D_2})(\cdot,\ell_i)\rangle\kappa_1(z_j)\kappa_2(z_j)}, \\
\qquad\text{for } \{_{j\in\{1,\ldots,|Z_1|\times|Z_2|\}}^{i\in\{1,\ldots,|I|\}}
\end{cases}
\end{aligned} \tag{37}$$

where $(C^{(I,\xi)}_{Z_1,Z_2})_{i,j}$ is the cost of assigning the jth measurement to track ℓ_i.

The first part and the second part of the cost matrix are the cost of assigning the measurement only from the first sensor and the second sensor, respectively, to the track. The third part is of the cost matrix is the cost of assigning the measurement both from the two sensors to the track.

The combined costs of every measurement to target assignments can be used to represent the cost of an assignment matrix which can be written as the Frobenius inner product

$$\mathrm{tr}(S^T C^{(I,\xi)}_{Z_1,Z_2}) = \sum_{i=1}^{|I|}\sum_{j=1}^{|(Z_1,Z_2)|} (C^{(I,\xi)}_{Z_1,Z_2})_{i,j} S_{i,j} \tag{38}$$

Substituting (32) into (36), it follows that

$$\eta^{(\xi,(\theta_1,\theta_2))}_{Z_1,Z_2}(\ell) = \begin{cases} \dfrac{\langle p^{(\xi)}(\cdot,\ell), p_{D_1}(,\ell) g_1(z_{\theta_1(\ell)}|,\ell) p_{D_2}(\cdot,\ell) g_2(z_{\theta_2(\ell)}|\cdot,\ell)\rangle}{\kappa_1(z_{\theta_1(\ell)})\kappa_2(z_{\theta_2(\ell)})}, \\ \quad \text{if } \begin{cases}\theta_1(\ell)>0\\ \theta_2(\ell)>0\end{cases} \\ \dfrac{\langle p^{(\xi)}(\cdot,\ell), p_{D_1}(\cdot,\ell) g_1(z_{\theta_1(\ell)}|\cdot,\ell)(1-p_{D_2}(\cdot,\ell))\rangle}{\kappa_1(z_{\theta_1(\ell)})}, \\ \quad \text{if } \begin{cases}\theta_1(\ell)>0\\ \theta_2(\ell)=0\end{cases} \\ \dfrac{\langle p^{(\xi)}(\cdot,\ell), (1-p_{D_1}(\cdot,\ell)) p_{D_2}(\cdot,\ell) g_2(z_{\theta_2(\ell)}|\cdot,\ell)\rangle}{\kappa_2(z_{\theta_2(\ell)})}, \\ \quad \text{if } \begin{cases}\theta_1(\ell)=0\\ \theta_2(\ell)>0\end{cases} \\ \langle p^{(\xi)}(\cdot,\ell), (1-p_{D_1}(\cdot,\ell))\cdot(1-p_{D_2}(\cdot,\ell))\rangle, \\ \quad \text{if } \begin{cases}\theta_1(\ell)=0\\ \theta_2(\ell)=0\end{cases} \end{cases} \tag{39}$$

Then

$$\begin{aligned}[\eta^{(\xi,(\theta_1,\theta_2))}_{Z_1,Z_2}(\ell)]^I &= \prod_{\ell\in I} \eta^{(\xi,(\theta_1,\theta_2))}_{Z_1,Z_2}(\ell) \\ &= \prod_{\substack{\theta_1(\ell)>0\\ \theta_2(\ell)>0}} \eta^{(\xi,(\theta_1,\theta_2))}_{Z_1,Z_2}(\ell) \prod_{\substack{\theta_1(\ell)>0\\ \theta_2(\ell)=0}} \eta^{(\xi,(\theta_1,\theta_2))}_{Z_1,Z_2}(\ell) \\ &\quad \times \prod_{\substack{\theta_1(\ell)=0\\ \theta_2(\ell)>0}} \eta^{(\xi,(\theta_1,\theta_2))}_{Z_1,Z_2}(\ell) \prod_{\substack{\theta_1(\ell)=0\\ \theta_2(\ell)=0}} \eta^{(\xi,(\theta_1,\theta_2))}_{Z_1,Z_2}(\ell) \end{aligned} \tag{40}$$

The cost is related to the filter hypothesis weight $\omega^{(I,\xi,(\theta_1,\theta_2))}(Z_1,Z_2) \propto \omega^{(I,\xi)}[\eta^{\xi,(\theta_1,\theta_2)}_{Z_1,Z_2}]^I$ by

$$\begin{aligned}[\eta^{(\xi,(\theta_1,\theta_2))}_{Z_1,Z_2}(\ell)]^I = \exp(-\mathrm{tr}(S^T C^{(I,\xi)}_{Z_1,Z_2})) \prod_{\ell\in I} \langle p^{(\xi)}(\cdot,\ell), (1-p_{D_1}) \\ \times(\cdot,\ell)(1-p_{D_2})(\cdot,\ell)\rangle \end{aligned} \tag{41}$$

The ranked assignment problem can be used to choose the least cost assignment matrices. The optimal assignment algorithm with cost matrix $C^{(I,\xi)}_{Z_1,Z_2}$ can generate an enumeration of association maps in non-decreasing order of $[\eta^{(\xi,(\theta_1,\theta_2))}_{Z_1,Z_2}(\ell)]^I$ and hence weights $\omega^{(I,\xi,(\theta_1,\theta_2))}(Z_1,Z_2) \propto \omega^{(I,\xi)}[\eta^{\xi,(\theta_1,\theta_2)}_{Z_1,Z_2}]^I$. Murty's algorithm is used in this paper to solve the ranked assignment problem [72]. An efficient algorithm for truncating the GLMB filtering density based on Gibbs sampling can be found in [42]. Even though the implementation proposed in [42] is more efficient than the Murty's algorithm used in this paper, the goals of this paper are the demonstration of tracking of space debris outside the observation volume and tracking with a multi-sensor network.

D. UPDATING PARAMETERS

For linear Gaussian multi-target models, $p_{D_1}(x,\ell) = p_{D_1}$, $p_{D_2}(x,\ell) = p_{D_2}$, $g(z|x,\ell) = \mathcal{N}(z; Hx, R)$, where H and R are the observation matrix and the observation noise covariance, respectively. A linear Gaussian multi-target model is used to represent the single target density $p^{(\xi)}(\cdot,\ell)$:

$$\sum_{i=1}^{J^{(\xi)}(\ell)} \omega^{(\xi)}_i(\ell)\mathcal{N}(x; m^{(\xi)}_i(\ell), P^{(\xi)}_i(\ell)) \tag{42}$$

For $i \in \{1,\ldots,|I|\}, j \in \{1,\ldots,|Z_s|\}$,where s denotes which sensor is used, the cost is

$$(C^{(I,\xi)}_{Z_1,Z_2})_{i,j} = -\ln\left(\frac{p_{D_s}\sum_{k=1}^{J^{(\xi)}(\ell_i)} \omega^{(\xi)}_k(\ell_i) q^{(\xi)}_k(z_{sj};\ell_i)}{(1-p_{D_s})\kappa_s(z_{sj})}\right) \tag{43}$$

The updated association history is

$$\eta^{(\xi,\theta_s)}_{Z_s}(\ell) = \sum_{i=1}^{J^{(\xi)}(\ell)} \omega^{(\xi,\theta_s)}_{Z_s,i}(\ell) \tag{44}$$

The updated location density is

$$p^{(\xi,\theta_s)}(x,\ell|Z_s) = \sum_{i=1}^{J^{(\xi)}(\ell)} \frac{\omega^{(\xi,\theta_s)}_{Z_s,i}(\ell)}{\eta^{(\xi,\theta_s)}_{Z_s}(\ell)} \mathcal{N}(x; m^{(\xi,\theta_s)}_{Z_s,i}(\ell), P^{(\xi,\theta_s)}_{s,i}(\ell)) \tag{45}$$

where

$$\begin{aligned} q^{(\xi)}_i(z_s;\ell) &= \mathcal{N}(z_s; H_s m^{(\xi)}_i(\ell), H_s P^{(\xi)}_i(\ell) H_s^T + R_s) \\ \omega^{(\xi,\theta_s)}_{Z_s,i}(\ell) &= \omega^{(\xi)}_i(\ell) \begin{cases} \dfrac{p_{D_s} q^{(\xi)}_i(z_{\theta_s(\ell)};\ell)}{\kappa_s(z_{\theta_s(\ell)})}, & \text{if } \theta_s(\ell)>0 \\ (1-p_{D_s}), & \text{if } \theta_s(\ell)=0 \end{cases} \\ P^{(\xi,\theta_s)}_{s,i} &= [I - K^{(\xi,\theta_s)}_{s,i}(\ell) H_s] P^{(\xi)}_i(\ell), \\ K^{(\xi,\theta_s)}_{s,i}(\ell) &= \begin{cases} P^{(\xi)}_i(\ell) H_s^T [H_s P^{(\xi)}_i(\ell) H_s^T + R_s]^{-1}, \\ \quad \text{if } \theta_s(\ell)>0 \\ 0, \quad \text{if } \theta_s(\ell)=0 \end{cases} \\ m^{(\xi,\theta_s)}_{Z_s,i}(\ell) &= \begin{cases} m^{(\xi)}_i(\ell) + K^{(\xi,\theta_s)}_{s,i}(\ell)(z_{\theta_s(\ell)} - H_s m^{(\xi)}_i(\ell)), \\ \quad \text{if } \theta_s(\ell)>0 \\ m^{(\xi)}_i(\ell), \quad \text{if } \theta_s(\ell)=0 \end{cases} \end{aligned}$$

For $i \in \{1,\ldots|I|\}, j \in \{1,\ldots,|Z_1|\times|Z_2|\}$, the cost is

$$(C^{(I,\xi)}_{Z_1,Z_2})_{i,j} = -\ln\left(\frac{p_{D_2} p_{D_1}\sum_{k=1}^{J^{(\xi)}(\ell_i)} \omega^{(\xi)}_k(\ell_i) q^{(\xi)}_k(z_{1j}z_{2j};\ell_i)}{(1-p_{D_1})(1-p_{D_2})\kappa_1(z_{1j})\kappa_2(z_{2j})}\right) \tag{46}$$

The updated association density is

$$\eta_{Z_1\times Z2}^{(\xi,\theta_1\times\theta_2)}(\ell)=\sum_{i=1}^{J^{(\xi)}(\ell)}\omega_{Z_1\times Z_2,i}^{(\xi,\theta_1\times\theta_2)}(\ell) \tag{47}$$

The updated location density is

$$p^{(\xi,\theta_1\times\theta_2)}(x,\ell|Z_1\times Z_2)=\sum_{i=1}^{J^{(\xi)}(\ell)}\frac{\omega_{Z_1\times Z_2,i}^{(\xi,\theta_1\times\theta_2)}(\ell)}{\eta_{Z_1\times Z_2}^{(\xi,\theta_1\times\theta_2)}(\ell)}\mathcal{N}(x;m_{Z_1\times Z_2,i}^{(\xi,\theta_1\times\theta_2)}(\ell),P_{Z_1\times Z_2,i}^{(\xi,\theta_1\times\theta_2)}(\ell)) \tag{48}$$

where

$$\begin{aligned}q_i^{(\xi)}(z_{1j}z_{2j};\ell_i)&=q_i^{(\xi)}(z_{1j};\ell_i)q_i^{(\xi)}(z_{2j};p^{(\xi,\theta_1)}(x,\ell_i|Z_1))\\&=\mathcal{N}(z_{1j};H_1m_i^{(\xi)}(\ell_i),H_1P_i^{(\xi)}(\ell_i)H_1^T+R_1)\\&\quad\cdot\mathcal{N}(z_{2j};H_2m_{Z_1,k}^{(\xi,\theta_1)}(\ell_i),H_2P_i^{(\xi,\theta_1)}H_2^T+R_2)\end{aligned}$$

$$\omega_{Z_1\times Z_2,i}^{(\xi,\theta_1\times\theta_2)}(\ell)=\omega_i^{(\xi)}(\ell)\begin{cases}\dfrac{p_{D_1}p_{D_2}q_i^{(\xi)}(z_{\theta_1(\ell)}z_{\theta_2(\ell)};\ell)}{\kappa_1(z_{\theta_1(\ell)})\kappa_2(z_{\theta_2(\ell)})} & \text{if }\begin{matrix}\theta_1(\ell)>0\\\theta_2(\ell)>0\end{matrix}\\(1-p_{D_1})(1-p_{D_2}) & \text{if }\begin{matrix}\theta_1(\ell)=0\\\theta_2(\ell)=0\end{matrix}\end{cases}$$

$$P_{Z_1\times Z_2,i}^{(\xi,\theta_1\times\theta_2)}=[I-K_{Z_1\times Z_2,i}^{(\xi,\theta_1\times\theta_2)}(\ell)H_2]P_i^{(\xi,\theta_1)}(\ell)$$

$$m_{Z_1\times Z_2,i}^{(\xi,\theta_1\times\theta_2)}(\ell)=\begin{cases}m_{Z_1,i}^{(\xi,\theta_1)}(\ell)+K_i^{(\xi,\theta_1\times\theta_2)}(\ell)(z_{\theta_2(\ell)}\\\qquad-H_2m_{Z_1,i}^{(\xi,\theta_1)}(\ell))\\m_i^{(\xi)}(\ell).\end{cases}$$

$$K_{Z_1\times Z_2,i}^{(\xi,\theta_1\times\theta_2)}(\ell)=\begin{cases}P_i^{(\xi,\theta_1)}(\ell)H_2^T[H_2P_i^{(\xi,\theta_1)}(\ell)H_2^T+R_2]^{-1},\\\qquad\text{if }\begin{matrix}\theta_1(\ell)>0\\\theta_2(\ell)>0\end{matrix}\\0,\quad\text{if }\begin{matrix}\theta_1(\ell)=0\\\theta_2(\ell)=0\end{matrix}\end{cases}$$

If the measurement model parameters are a function of the label ℓ, $p_D=p_D(\ell)$, $H=H(\ell)$, $R=R(\ell)$ can be substituted into the above equations.

E. THE EM ALGORITHM FOR UPDATING WITH NON-UNIFORM DETECTION PROBABILITY

The multi-sensor δ-GLMB filter is performed on the assumption that all sensors have the same observation volume. Normally, a δ-GLMB filter with uniform detection probability does not provide any information for targets outside of its observation volume because no measurements are available. However, since the observation model only affects the prediction, not the update, estimation of targets can still be provided because the prediction is always available. We set the detection probability to zero for areas outside of the observation volume in this paper. p_{Din} and p_{Dout} are used to represent the detection probability for inside and outside of the observation volume, respectively. A similar approach for space object tracking in a limited field of view was proposed in [73].

We assume that the single-target density is a Gaussian mixture when computing the parameters. Since UKF is used in this paper for the space debris transition function, each Gaussian item is represented by a set of sigma-points. If all sigma-points are inside or outside the observation volume, the detection probability for this Gaussian item is set to p_{Din} and p_{Dout}, respectively. Otherwise, the EM algorithm is used to build a new GM to approximate the predicted densities inside and outside of the observation volume.

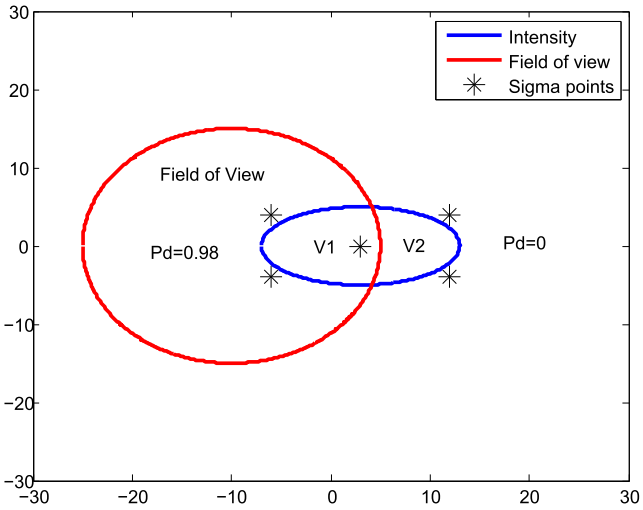

FIGURE 1. The predicted intensity function is shown by a GM. The blue circle is one Gaussian item. V1 represents the part inside the observation volume and V2 represents the outside part.

An illustration of this scenario is shown in figure 1. The predicted intensity function is shown by a GM. The blue circle is one Gaussian item. V1 represents the part inside the observation volume and V2 represents the outside part.

The EM algorithm is an efficient method to find the maximum-likelihood estimate of the unknown parameters of an underlying distribution from a given data set. Usually, the data set has missing values or is incomplete. Each iteration of the EM algorithm has two procedures: The Expectation step (E-step) and the Maximization step (M-step). The E-step creates a function for the expectation of the log-likelihood evaluated using the current estimate for the parameters. In the M-step, the likelihood function is maximized under the assumption that the missing data are known.

If the sigma-points of one Gaussian item are on both sides of the observation edge, then $N=1000$ points are sampled from this Gaussian distribution. Depending on whether the points are inside the observation volume or not, these points are divided into two groups: $Points_{in}$ and $Points_{out}$. The EM algorithm is used for Gaussian mixture parameter estimation. Each Gaussian item is represented by two new Gaussian mixtures, i.e.:

$$\begin{aligned}&\sum_{i=1}^{J^{(\xi)}(\ell)}\omega_i^{(\xi)}(\ell)\mathcal{N}(x;m_i^{(\xi)}(\ell),P_i^{(\xi)}(\ell))\\&\quad=\sum_{i=1}^{J^{(\xi)}(\ell)}\omega_i^{(\xi)}(\ell)\Big(\sum_{h=1}^{H^{(\xi)}(\ell)}\omega_h^{(\xi)}(\ell)\mathcal{N}(x;m_h^{(\xi)}(\ell),P_h^{(\xi)}(\ell))\\&\quad+\sum_{k=1}^{K^{(\xi)}(\ell)}\omega_k^{(\xi)}(\ell)\mathcal{N}(x;m_k^{(\xi)}(\ell),P_k^{(\xi)}(\ell))\Big)\end{aligned}$$

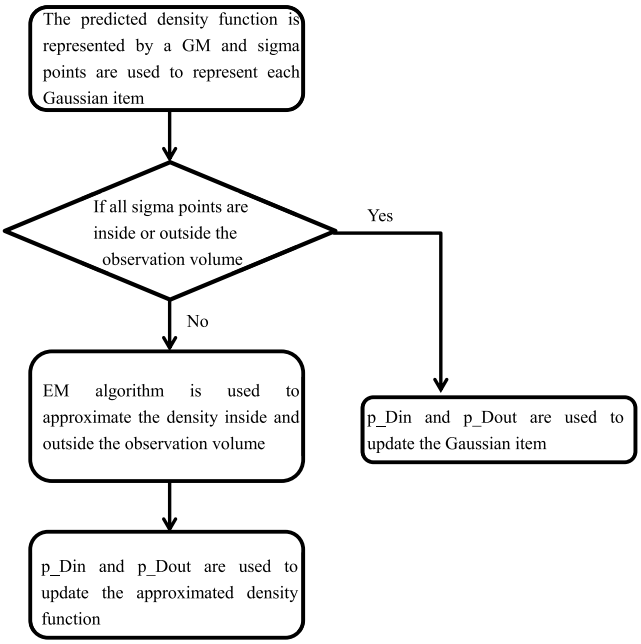

FIGURE 2. Estimation for objects inside and outside the observation volume.

This new Gaussian mixture then can be used in the δ-GLMB update. An illustration of the method is shown in figure 2.

The parameters in the density approximation include the number of Gaussian items, the weights, the covariance matrices, and the means which are chosen as follows.

(1) The number of the Gaussian components: It is very difficult to derive the number of Gaussian components even though it is very important. In practice, a reasonably large number ($J_{max} = 10$ in this paper) is chosen as the maximum number of new Gaussian items in the approximation. The EM algorithm is used for situations with a different number of Gaussian components ($J_{min} = 1, \ldots, J_{max} = 10$). Then the Bayesian information criterion (BIC) is used to determine the best number of Gaussian components. The BIC is a criterion for model selection among a finite set of models.
Using the estimation of targets outside of the observation volume, the proposed multi-sensor δ-GLMB can be used for sensors with different observation volumes [74]. The model with the lowest BIC is chosen. BIC is defined as follows:

$$BIC(J, \theta, P) = -2log\ L(\theta, J|P) + M\ ln(N)$$

where J is the number of Gaussian items, θ is the estimated parameters which maximize the likelihood function, P is the sampled data, $L(\cdot)$ is the maximized value of the likelihood function, M is the number of parameters estimated and N is the number of sampled points.

(2) The weights for the Gaussian items are the same and set as $W_j = \frac{1}{J}$.

(3) The means of Gaussian position components can be chosen by uniformly sampling the observation volume. And the means of Gaussian velocity components can be set to zeros.

F. MEASUREMENT-BASED BIRTH MODEL

A birth model is required in space debris tracking in a similar way to initial orbit determination when initiating new targets. If background knowledge about the environment of the system is known, the birth-model can be built with fixed-birth locations and small spatial uncertainties. Since fixed-birth locations minimize the incidence of false tracks, they are beneficial in scenarios with high clutter rate. In most space debris tracking scenarios, prior information of space debris locations is not available. Consequently, a measurement-based birth model is required for δ-GLMB filtering.

An adaptive birth model for Gaussian mixture PHD and CPHD filtering was proposed in [75]. The adaptive birth distributions for δ-GLMB filtering should also concentrate around measurements not originating from existing tracks. The birth distribution at time step k depends on the measurements at time step $k-1$ and is denoted by

$$\boldsymbol{\pi}_{B,k} = \left\{r^{(\ell)}_{B,k-1}(z), p^{(\ell)}_{B,k-1}(x|z)\right\}^{|Z_{k-1}|}_{\ell=1}$$

where $p^{(\ell)}_{B,k-1}(x|z)$ denotes the probability density of birth track ℓ and $r^{(\ell)}_{B,k-1}(z)$ is its weight. The probability density is represented by a Gaussian item in this paper. Since bearings and range measurements are used in this paper, measurement can be used to calculate target positions in the X, Y and Z directions and used as the mean values for birth positions. Mean values for velocities are set to zero. The values for the covariance are based on experience. A small value results in faster track confirmation but can lead to lost tracks. A large value results in slower track confirmation but can generally initiate new tracks.

G. SYNCHRONIZATION AND INCONSISTENCY

Multi-sensor tracking systems suffer from the problem of synchronization and inconsistency. It becomes more difficult to achieve synchronization as the number of nodes in the system increases. The effect of communication delay becomes more severe in larger multi-sensor networks. Even small time delays can deteriorate the performance of the system or even destabilize it. Coordination can be achieved for the discrete-time delayed systems with linear dynamics [76]. The output synchronization of nonlinear systems with communication time delays was discussed in [77]. A new framework was proposed in [78] to address the synchronization of complex networks.

V. NUMERICAL RESULTS

We demonstrate the efficacy of multi-sensor δ-GLMB to track space debris through three experiments. The first experiment shows that the proposed δ-GLMB filter can provide estimation for targets outside of the observation volume.

The second experiment shows the δ-GLMB tracking performance for sensors with complementary observation volumes. The third experiment shows that the multi-sensor δ-GLMB filter significantly improves the tracking performance over single sensor δ-GLMB filtering and the centralized CPHD filter. Three sensors with complementary observation volumes are used in the second experiment. Sensors in The target state can be represented by a vector, $x_k = [p_x\ p_y\ p_z\ v_x\ v_y\ v_z]^T$ with position and velocity on x, y and z direction. The state transition model is:

$$x_{k+1} = f(x_k) + w_k$$

The transition density function is obtained with the help of Turboprop and is denoted by $f(\cdot)$. $w_k \sim N(\cdot; 0, Q)$ is the transition process noise with $Q = diag([\sigma_{px}^2, \sigma_{py}^2, \sigma_{pz}^2, \sigma_{vx}^2, \sigma_{vy}^2, \sigma_{vz}^2])$, $\sigma_{px} = \sigma_{py} = \sigma_{pz} = 1$ km, $\sigma_{vx} = \sigma_{vy} = \sigma_{vz} = 0.01\ km/s$. The birth model to generate the simulation scenario is a Labeled Multi-Bernoulli RFS with parameters $\pi_B = \{r_B^{(i)}, p_B^{(i)}\}_{i=1}^5$ where $r_B^{(i)} = 0.02$ and $p_B^{(i)}(x) = \mathcal{N}(x; m_B^{(i)}, P_B)$ with

$$\begin{aligned}
m_\gamma^{(1)} &= [8368.9\,km, -191.1\,km, 0.0217\,km, \\
&\quad 0.1577\,km/s, 6.8986\,km/s, 0\,km/s]^T \\
m_\gamma^{(2)} &= [8386.9\,km, -236.09\,km, -111.47\,km, \\
&\quad 0.214\,km/s, 5.966\,km/s, 3.448\,km/s]^T \\
m_\gamma^{(3)} &= [8406.9\,km, -201.6\,km, -166.6\,km, \\
&\quad 0.2134\,km/s, 4.8651\,km/s, 4.8658\,km/s]^T \\
m_\gamma^{(4)} &= [8347.8\,km, -208.9\,km, 95.56\,km, \\
&\quad 0.1894\,km/s, 5.9807\,km/s, -3.4534\,km/s]^T \\
m_\gamma^{(5)} &= [8326.6\,km, -206.24\,km, 170.8\,km, \\
&\quad 0.2216\,km/s, 4.889\,km/s, -4.889\,km/s]^T \\
P_\gamma &= diag([10\,km, 10\,km, 10\,km, \\
&\quad 0.01\,km/s, 0.01\,km/s, 0.01\,km/s])
\end{aligned}$$

Note that the birth model is only used to generate target trajectories and this information is not available to nodes.

A Poisson RFS with intensity $\kappa_k(z) = \lambda_c V u(z)$ is used to model the clutter. The uniform density over the observation volume is denoted by $u(\cdot)$, V is the "volume", and λ_c is the average number of clutter returns per unit volume, 400 in this paper.

In the demonstration, the observation task is performed with three nodes. The sensor's observation is a noisy bearing and range vector given by

$$z_k = \begin{bmatrix} \sqrt{p_{x,k}^2 + p_{y,k}^2 + p_{z,k}^2} \\ \arctan\left(\dfrac{p_{y,k}}{p_{x,k}}\right) \\ \arctan\left(\dfrac{p_{z,k}}{\sqrt{p_{x,k}^2 + p_{y,k}^2}}\right) \end{bmatrix} + \varepsilon_k$$

where $\varepsilon_k \sim N(\cdot; 0, R_k)$ with

$$\begin{aligned}
R_{k1} &= diag([\sigma_{r1}^2, \sigma_{\alpha1}^2, \sigma_{\beta1}^2]), \\
\sigma_{r1} &= 0.12\ km, \sigma_{\alpha1} = 0.02^\circ \quad \sigma_{\beta1} = 0.01^\circ \\
R_{k2} &= diag([\sigma_{r2}^2, \sigma_{\alpha2}^2, \sigma_{\beta2}^2]), \\
\sigma_{r2} &= 0.22\ km, \sigma_{\alpha2} = 0.01^\circ \quad \sigma_{\beta2} = 0.01^\circ \\
R_{k3} &= diag([\sigma_{r3}^2, \sigma_{\alpha3}^2, \sigma_{\beta3}^2]), \\
\sigma_{r3} &= 0.05\ km, \sigma_{\alpha3} = 0.02^\circ \quad \sigma_{\beta3} = 0.02^\circ
\end{aligned}$$

$\Delta = 1s$ is the sampling period. The detection probability inside the observation volume $p_{Din} = 0.98$. The survival probability for the first and the second experiment is $p_{S1} = 0.999$ and $p_{S2} = 0.99$, respectively.

The δ-GLMB filter is capped to 10000 components. Results are shown over 100 Monte Carlo trials. The Optimal Sub-Pattern Assignment (OSPA) metric is used to evaluate the performance [79]. OSPA is a mathematically consistent metric used for performance evaluation in multi-object tracking situations. The Euclidean distance is set to $p = 2$ and the cutoff parameter is set to $c = 1.5\,km$ in this paper.

A. SINGLE SENSOR WITH LIMITED OBSERVATION VOLUME

This experiment is to show that the δ-GLMB filter with detection probability set to zero outside the observation volume can provide estimation for targets when they go outside the observation volume. Five targets are presented here as an example. The observation region for node1 is $V1 = [0\ 2800]\,km \times [-10^\circ\ 15^\circ] \times [-10^\circ\ 10^\circ]$. The estimation for δ-GLMB with uniform detection probability setting is shown in Figure 3a. The estimation for δ-GLMB with detection probability set to zero outside the observation volume is shown in Figure 3a. The solid blue lines represent the true tracks and the black dots represent the estimations.

It can be seen that both filters provide accurate estimation for targets inside the observation volume. However δ-GLMB with uniform detection probability setting does not provide estimation for targets outside of the observation volume while the δ-GLMB proposed in this paper can.

When the δ-GLMB filter has a uniform detection probability setting, there is no estimation for the target if there is no measurement captured. Because there is no measurement to update the prediction, the weight for the corresponding item will drop and the filter will assume that the target dies. With the detection probability setting and the EM algorithm used in this paper, when the target goes outside the observation volume and there is no measurement available, the prediction part can be preserved and the estimation is essentially the prediction.

B. CENTRALIZED δ-GLMB TRACKING FOR SENSORS WITH COMPLEMENTARY OBSERVATION VOLUMES

This subsection is to show the effectiveness of centralized δ-GLMB Tracking for sensors with complementary observation volumes. Fusion algorithms with uniform detection

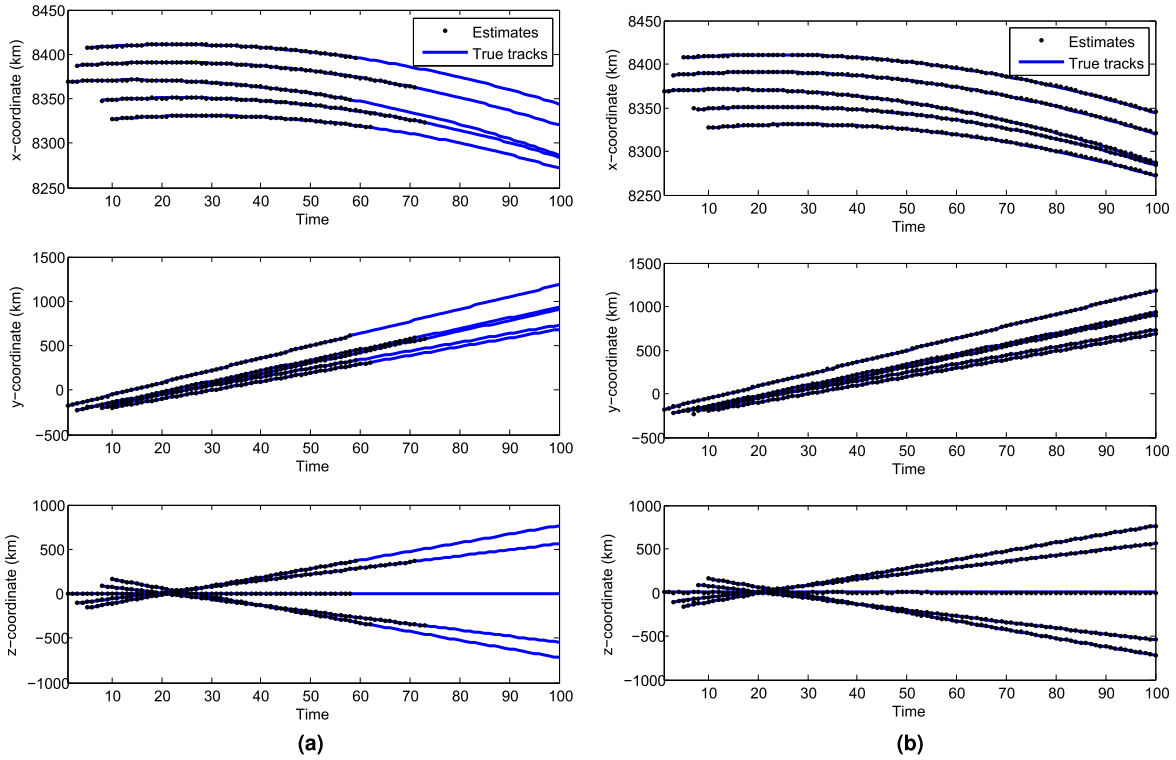

FIGURE 3. δ-GLMB estimation with different detection probability setting. (a) δ-GLMB estimation with uniform detection probability. Estimation is only provided for targets inside the observation volume. (b) δ-GLMB with detection probability set to zero outside the observation volume. Estimation is also available for targets outside the observation volume.

probability settings must consider the observation volume overlaps, which makes the fusion much more difficult when more sensors are used. With the approach used in this paper, estimation for objects outside the observation volume is available. Then the fusion can be performed in the same way as for sensors with the same observation volume.

Three sensors observing from the same location are used in this experiment. The location is $L = (0°, 0°)$. The observation volumes for the three sensors are

$$V1 = [0\ 2800]\,km \times [-10°\ 15°] \times [-30°\ 30°]$$
$$V2 = [0\ 2800]\,km \times [15°\ 25°] \times [-30°\ 30°]$$
$$V3 = [0\ 2800]\,km \times [25°\ 35°] \times [-30°\ 30°]$$

This ensures that all of the space debris is inside the combined observation volume of all of the sensors. The OSPA performance of a single sensor and the centralized system are shown in figure 4. This figure shows that a single sensor δ-GLMB can provide good estimation for objects when they are inside the observation volume. However, the estimation results are poor when there are no measurements for objects outside of the observation volume and only the prediction model is available. Since all of the space debris is in the combined observation volumes of all sensors, the tracking performance from centralized δ-GLMB can provide good estimation all the time.

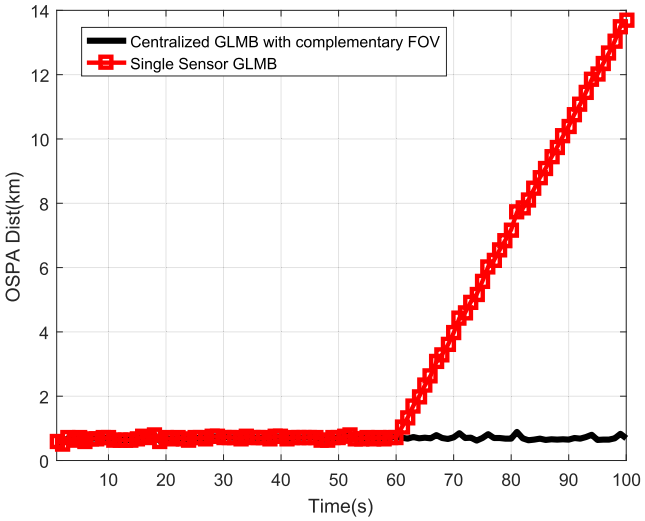

FIGURE 4. OSPA distance for single sensor δ-GLMB filtering and centralized δ-GLMB filtering with complementary observation volumes.

C. MULTI-SENSOR δ-GLMB TRACKING FOR SENSORS WITH SIMILAR OBSERVATION VOLUMES

This experiment is to show that the multi-sensor δ-GLMB can significantly improve the tracking performance. All three nodes are on the surface of the Earth. The latitude and longitude of node1, node2 to node3 are

$$L1 = (0°, 0°), \quad L2 = (30°N, 0°), \quad L3 = (30°S, 0°),$$

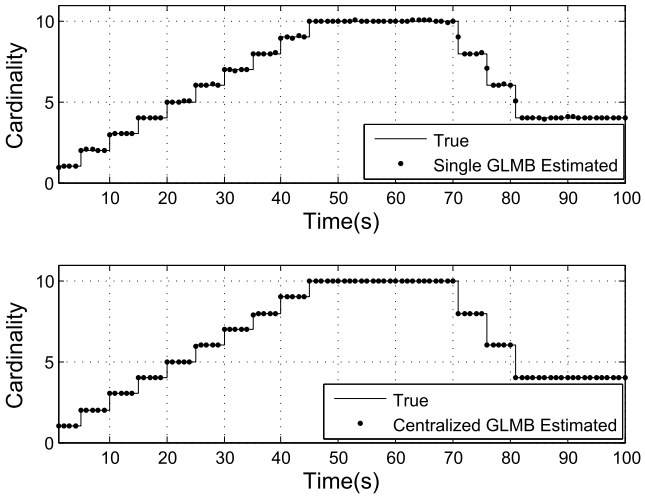

FIGURE 5. Cardinality estimation from single δ-GLMB filtering and centralized δ-GLMB filtering with similar observation volumes.

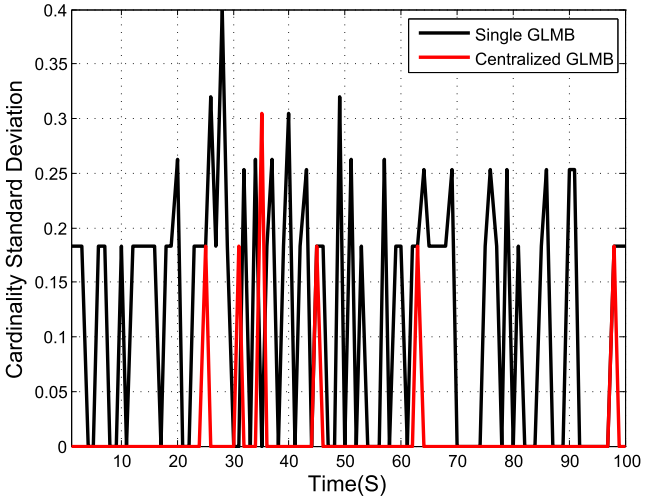

FIGURE 6. Cardinality estimation standard deviation for single δ-GLMB filtering and centralized δ-GLMB filtering with similar observation volumes.

respectively. Node1 is on the x-z plane initially. All three nodes rotate with the Earth. The surveillance regions for node1, node2 and node3 in this experiment are:

$$V1 = [0\ 2800]\,km \times [-10^\circ\ 15^\circ] \times [-10^\circ\ 10^\circ]$$
$$V2 = [0\ 4500]\,km \times [-10^\circ\ 15^\circ] \times [-88^\circ\ -65^\circ]$$
$$V3 = [0\ 4500]\,km \times [-10^\circ\ 15^\circ] \times [65^\circ\ 85^\circ]$$

respectively.

The mean values of the cardinality estimation for single sensor δ-GLMB filtering and the centralized δ-GLMB filtering are shown in Figure 5. We can see that both filters show good performance for cardinality estimation.

The standard deviations for single sensor δ-GLMB filtering and the centralized δ-GLMB filtering are shown in figure 6 and show that the estimated cardinality variance

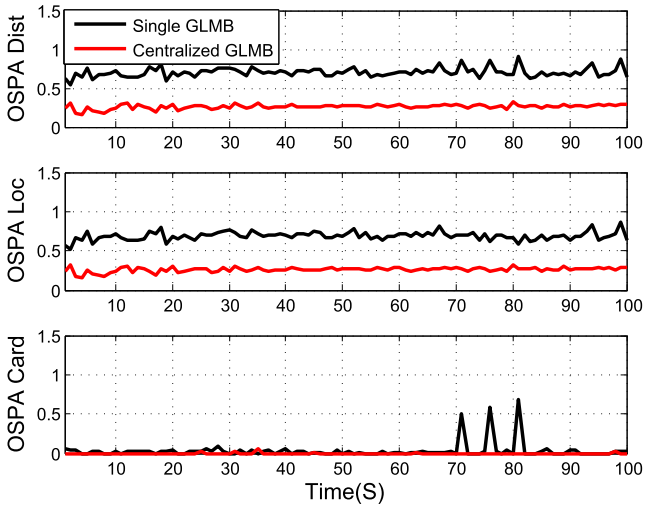

FIGURE 7. OSPA distance for single δ-GLMB and centralized δ-GLMB with similar observation volumes and their localization and cardinality components.

performance from the centralized δ-GLMB filtering is better than the single sensor δ-GLMB filtering.

The OSPA distance for single sensor δ-GLMB filtering and centralized δ-GLMB filtering are shown in figure 7. It is shown in the figure that multi-sensor δ-GLMB filtering outperforms the single sensor δ-GLMB filtering on the overall miss distance and on both the localization and cardinality components.

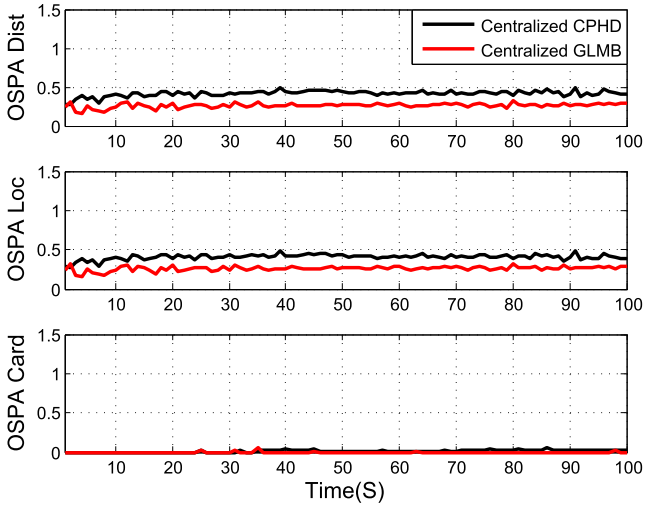

FIGURE 8. OSPA distance for single centralized CPHD and centralized δ-GLMB and their localization and cardinality components.

The comparison between centralized CPHD filtering and centralized δ-GLMB filtering is shown in figure 8. It can be seen that the centralized δ-GLMB filter shows much better performance than the centralized CPHD filter on the overall miss distance. Both filters show very good performance on the cardinality component. The centralized δ-GLMB filter outperforms the centralized CPHD filter on

the localization component. The improved localization performance is attributed to two factors: (a) the δ-GLMB filter can better localize targets because of a more accurate filtering density propagation, and (b) the spooky effect of CPHD: when a target is undetected, the PHD mass in this vicinity is shifted to the vicinity of the detected targets.

VI. CONCLUDING REMARKS

This paper details the implementation of a multi-sensor δ-GLMB filter for space debris tracking. This proposed algorithm is general enough to accommodate non-linear target dynamics, clutter intensity, non-uniform detection probability and unknown and time-varying number of targets. The key innovation lies in the numerical implementation of the centralized δ-GLMB update and the truncation of densities without exhaustively computing all the components. The proposed algorithm can provide state information for targets outside of the observation volume. Experiments confirm that the proposed system shows excellent performance for multi-sensor space debris tracking. The space-debris tracking problem is of concern to all countries. While it is clear that organizations with significant resources can afford to use a centralized system, the method proposed in this paper is less resource intensive.

REFERENCES

[1] J. A. Kennewell and B.-N. Vo, "An overview of space situational awareness," in *Proc. 16th Int. Conf. Inf. Fusion*, Jul. 2013, pp. 1029–1036.
[2] B. A. Jones, D. S. Bryant, B.-T. Vo, and B.-N. Vo, "Challenges of multi-target tracking for space situational awareness," in *Proc. 18th Int. Conf. Inf. Fusion (Fusion)*, Jul. 2015, pp. 1278–1285.
[3] B. A. Jones and A. Doostan, "Satellite collision probability estimation using polynomial chaos expansions," *Adv. Space Res.*, vol. 52, no. 11, pp. 1860–1875, Dec. 2013.
[4] M. Hechler and J. C. Van der Ha, "Probability of collisions in the geostationary ring," *J. Spacecraft Rockets*, vol. 18, no. 4, pp. 361–366, 1981.
[5] R. Oliva, E. Blasch, and R. Ogan, "Applying aerospace technologies to current issues using systems engineering: 3rd AESS chapter summit," *IEEE Aerosp. Electron. Syst. Mag.*, vol. 28, no. 2, pp. 34–41, Feb. 2013.
[6] B. A. Jones and B.-N. Vo, "A labeled multi-bernoulli filter for space object tracking," in *Proc. AAS/AIAA Spaceflight Mech. Meeting*, Jan. 2014, pp. 11–15.
[7] B. A. Jones, A. Doostan, and G. H. Born, "Nonlinear propagation of orbit uncertainty using non-intrusive polynomial chaos," *J. Guid., Control, Dyn.*, vol. 36, no. 2, pp. 430–444, 2013.
[8] R. P. Mahler, *Statistical Multisource-Multitarget Information Fusion*. Norwood, MA, USA: Artech House, 2007.
[9] R. P. S. Mahler, *Advances in Statistical Multisource-Multitarget Information Fusion*. Norwood, MA, USA: Artech House, 2014.
[10] R. R. Juang, A. Levchenko, and P. Burlina, "Tracking cell motion using GM-PHD," in *Proc. IEEE Int. Symp. Biomed. Imag., From Nano Macro*, Jun./Jul. 2009, pp. 1154–1157.
[11] R. Hoseinnezhad, B.-N. Vo, B.-T. Vo, and D. Suter, "Visual tracking of numerous targets via multi-bernoulli filtering of image data," *Pattern Recognit.*, vol. 45, no. 10, pp. 3625–3635, Oct. 2012.
[12] S. H. Rezatofighi, S. Gould, B. T. Vo, B. N. Vo, K. Mele, and R. Hartley, "Multi-Target tracking with time-varying clutter rate and detection profile: Application to time-lapse cell microscopy sequences," *IEEE Trans. Med. Imag.*, vol. 34, no. 6, pp. 1336–1348, Jun. 2015.
[13] K. Y. K. Leung, F. Inostroza, and M. Adams, "Relating random vector and random finite set estimation in navigation, mapping, and tracking," *IEEE Trans. Signal Process.*, vol. 65, no. 17, pp. 4609–4623, Sep. 2017.
[14] G. Battistelli *et al.*, "Traffic intensity estimation via PHD filtering," in *Proc. Eur. Radar Conf.*, Amsterdam, The Netherlands, Oct. 2008, pp. 340–343.
[15] M. Canaud, L. Mihaylova, J. Sau, and N.-E. El Faouzi, "Probabilty hypothesis density filtering for real-time traffic state estimation and prediction," *Netw. Heterogeneous Media*, vol. 8, no. 3, pp. 825–842, 2013.
[16] D. Meissner, S. Reuter, and K. Dietmayer, "Road user tracking at intersections using a multiple-model PHD filter," in *Proc. IEEE Intell. Vehicles Symp. (IV)*, Jun. 2013, pp. 377–382.
[17] J. Mullane, B.-N. Vo, M. D. Adams, and B.-T. Vo, "A random-finite-set approach to Bayesian SLAM," *IEEE Trans. Robot.*, vol. 27, no. 2, pp. 268–282, Apr. 2011.
[18] F. Zhang, H. Stähle, A. Gaschler, C. Buckl, and A. Knoll, "Single camera visual odometry based on random finite set statistics," in *Proc. IEEE/RSJ Int. Conf. Intell. Robots Syst.*, Oct. 2012, pp. 559–566.
[19] C. S. Lee, D. E. Clark, and J. Salvi, "SLAM with dynamic targets via single-cluster PHD filtering," *IEEE J. Sel. Topics Signal Process.*, vol. 7, no. 3, pp. 543–552, Jun. 2013.
[20] N. T. Pham, W. Huang, and S. H. Ong, "Tracking multiple objects using probability hypothesis density filter and color measurements," in *Proc. IEEE Int. Conf. Multimedia Expo*, Jul. 2007, pp. 1511–1514.
[21] E. Maggio, M. Taj, and A. Cavallaro, "Efficient multitarget visual tracking using random finite sets," *IEEE Trans. Circuits Syst. Video Technol.*, vol. 18, no. 8, pp. 1016–1027, Aug. 2008.
[22] R. Hoseinnezhad, B.-N. Vo, and B.-T. Vo, "Visual tracking in background subtracted image sequences via multi-Bernoulli filtering," *IEEE Trans. Signal Process.*, vol. 61, no. 2, pp. 392–397, Jan. 2013.
[23] D. Clark, I. T. Ruiz, Y. Petillot, and J. Bell, "Particle PHD filter multiple target tracking in sonar image," *IEEE Trans. Aerosp. Electron. Syst.*, vol. 43, no. 1, pp. 409–416, Jan. 2007.
[24] X. Zhang, "Adaptive control and reconfiguration of mobile wireless sensor networks for dynamic multi-target tracking," *IEEE Trans. Autom. Control*, vol. 56, no. 10, pp. 2429–2444, Oct. 2011.
[25] J. Lee and K. Yao, "Initialization of multi-Bernoulli random-finite-sets over a sensor tree," in *Proc. ICASSP*, 2012, pp. 2689–2692.
[26] G. Battistelli, L. Chisci, C. Fantacci, A. Farina, and A. Graziano, "Consensus CPHD filter for distributed multitarget tracking," *IEEE J. Sel. Topics Signal Process.*, vol. 7, no. 3, pp. 508–520, Jun. 2013.
[27] M. Uney, D. E. Clark, and S. J. Julier, "Distributed fusion of PHD filters via exponential mixture densities," *IEEE J. Sel. Topics Signal Process.*, vol. 7, no. 3, pp. 521–531, Jun. 2013.
[28] C. Fantacci, B.-N. Vo, B.-T. Vo, G. Battistelli, and L. Chisci. (2015). "Consensus labeled random finite set filtering for distributed multi-object tracking." [Online]. Available: https://arxiv.org/abs/1501.01579
[29] L. Cament, M. Adams, J. Correa, and C. Perez, "The δ-generalized multi-Bernoulli poisson filter in a multi-sensor application," in *Proc. Int. Conf. Control, Automat. Inf. Sci. (ICCAIS)*, Oct./Nov. 2017, pp. 32–37.
[30] K. Y. K. Leung, F. Inostroza, and M. Adams, "Multifeature-based importance weighting for the PHD SLAM filter," *IEEE Trans. Aerosp. Electron. Syst.*, vol. 52, no. 6, pp. 2697–2714, Dec. 2016.
[31] A. F. Pareja, M. Adams, J. S. Sanchez, and M. T. Torriti, "Random finite sets in visual SLAM," Dept. Elect. Eng., Univ. Chile, Santiago, Chile, Tech. Rep., 2017.
[32] K. Y. K. Leung, F. Inostroza, and M. Adams, "Generalizing random-vector SLAM with random finite sets," in *Proc. IEEE Int. Conf. Robot. Automat. (ICRA)*, May 2015, pp. 4583–4588.
[33] J. Mullane, S. Keller, and M. Adams, "Random set versus vector based SLAM in the presence of high clutter," in *Proc. ICRA*, 2012, pp. 1–7.
[34] R. P. S. Mahler, "Multitarget Bayes filtering via first-order multitarget moments," *IEEE Trans. Aerosp. Electron. Syst.*, vol. 39, no. 4, pp. 1152–1178, Oct. 2003.
[35] B. N. Vo and W. K. Ma, "The Gaussian mixture probability hypothesis density filter," *IEEE Trans. Signal Process.*, vol. 54, no. 11, pp. 4091–4104, Nov. 2006.
[36] R. Mahler, "PHD filters of higher order in target number," *IEEE Trans. Aerosp. Electron. Syst.*, vol. 43, no. 4, pp. 1523–1543, Oct. 2007.
[37] B. T. Vo, B. N. Vo, and A. Cantoni, "Analytic implementations of the cardinalized probability hypothesis density filter," *IEEE Trans. Signal Process.*, vol. 55, no. 7, pp. 3553–3567, Jul. 2007.
[38] B.-T. Vo, B.-N. Vo, and A. Cantoni, "The cardinality balanced multi-target multi-Bernoulli filter and its implementations," *IEEE Trans. Signal Process.*, vol. 57, no. 2, pp. 409–423, Feb. 2009.
[39] B.-N. Vo, B.-T. Vo, N.-T. Pham, and D. Suter, "Joint detection and estimation of multiple objects from image observations," *IEEE Trans. Signal Process.*, vol. 58, no. 10, pp. 5129–5141, Oct. 2010.

[40] B.-T. Vo and B.-N. Vo, "Labeled random finite sets and multi-object conjugate priors," *IEEE Trans. Signal Process.*, vol. 61, no. 13, pp. 3460–3475, Jul. 2013.
[41] B. N. Vo, B. T. Vo, and D. Phung, "Labeled random finite sets and the Bayes multi-target tracking filter," *IEEE Trans. Signal Process.*, vol. 62, no. 24, pp. 6554–6567, Dec. 2014.
[42] B.-N. Vo, B.-T. Vo, and H. Hoang, "An efficient implementation of the generalized labeled multi-bernoulli filter," *IEEE Trans. Signal Process.*, vol. 65, no. 8, pp. 1975–1987, Apr. 2017.
[43] F. Papi, B.-N. Vo, B.-T. Vo, C. Fantacci, and M. Beard, "Generalized labeled multi-Bernoulli approximation of multi-object densities," *IEEE Trans. Signal Process.*, vol. 63, no. 20, pp. 5487–5497, Oct. 2015.
[44] S. Reuter, B. T. Vo, B. N. Vo, and K. Dietmayer, "The labeled multi-Bernoulli filter," *IEEE Trans. Signal Process.*, vol. 62, no. 12, pp. 3246–3260, Dec. 2014.
[45] A. Pak, J. Correa, and M. Adams, "Robust joint target detection and tracking for space situational awareness," *J. Guid., Control, Dyn.*, vol. 41, no. 1, pp. 119–136, 2017.
[46] I. I. Hussein, K. J. DeMars, C. Früh, R. S. Erwin and M. K. Jah, "An AEGIS-FISST integrated detection and tracking approach to space situational awareness," in *Proc. 15th Int. Conf. Inf. Fusion*, Jul. 2012, pp. 2065–2072.
[47] B. A. Jones, S. Gehly, and P. Axelrad, "Measurement-based birth model for a space object cardinalized probability hypothesis density filter," in *Proc. AIAA/AAS Astrodynamics Spec. Conf.*, 2014, p. 4311.
[48] W. Faber, S. Chakravorty, and I. I. Hussein, "A randomized sampling based approach to multi-object tracking," in *Proc. 18th Int. Conf. Inf. Fusion (Fusion)*, Jul. 2015, pp. 1307–1314.
[49] K. J. DeMars, J. S. McCabe, and J. E. Darling, "Collaborative multi-sensor tracking and data fusion," in *Proc. 5th AAS/AIAA Space Flight Mech. Meeting*, Jan. 2015, pp. 11–15.
[50] I. Hussein, K. DeMars, and C. Fruh, M. Jah, and R. Erwin, "An AEGIS-FISST algorithm for multiple object tracking in space situational awareness," in *Proc. AIAA/AAS Astrodynamics Spec. Conf.*, Aug. 2012, p. 4807.
[51] K. J. DeMars, I. I. Hussein, C. Frueh, M. K. Jah, and R. S. Erwin, "Multiple-object space surveillance tracking using finite-set statistics," *J. Guid., Control, Dyn.*, vol. 38, no. 9, pp. 1741–1756, 2015.
[52] W. Faber, S. Chakravorty, and I. I. Hussein. (2016). "Multi-object tracking with multiple birth, death, and spawn scenarios using a randomized hypothesis generation technique (R-FISST)." [Online]. Available: https://arxiv.org/abs/1603.07684
[53] I. I. Hussein, C. Früeh, R. Erwin, and M. K. Jah, "An aegis-fisst algorithm for joint detection, classification and tracking," in *Proc. AAS/AIAA Astrodynamics Spec. Conf.*, 2013, pp. 3599–3614.
[54] K. J. DeMars, I. I. Hussein, M. K. Jah, and R. S. Erwin, "The Cauchy-Schwarz divergence for assessing situational information gain," in *Proc. 15th Int. Conf. Inf. Fusion*, Jul. 2012, pp. 1126–1133.
[55] M. Adams, "Space object detection and tracking within a finite set statistics framework," Dept. Elect. Eng., Univ. de Chile, Santiago, Chile, Tech. Rep., 2017.
[56] B. Wei, B. D. Nener, W. Liu, and L. Ma, "Global tracking of space debris via CPHD and consensus," *Adv. Space Res.*, vol. 59, pp. 2548–2562, Mar. 2017.
[57] B. Wei and B. Nener, "Consensus labeled multi-bernoulli filtering for distributed space debris tracking," in *Proc. Int. Conf. Control, Automat. Inf. Sci. (ICCAIS)*, Oct./Nov. 2017, pp. 203–208.
[58] B. Wei and B. Nener, "Distributed space debris tracking with consensus labeled random finite set filtering," *Sensors*, vol. 18, no. 9, p. 3005, Sep. 2018.
[59] B. Weeden, P. Cefola, and J. Sankaran, "Global space situational awareness sensors," in *Proc. AMOS*, Maui, HI, USA, Sep. 2010, pp. 1–10.
[60] National Research Council; Division on Engineering and Physical Sciences; Aeronautics and Space Engineering Board; Committee for the Assessment of the U.S. Air Force's Astrodynamic Standards, *Continuing KeplerâĂŹs Quest: Assessing Air Force Space Command's Astrodynamics Standards*. Washington, DC, USA: National Academies Press, 2012.
[61] S. J. Julier, "Fusion without independence," in *Proc. IET Seminar Target Tracking Data Fusion, Algorithms Appl.*, Apr. 2008, pp. 3–4.
[62] S. J. Julier, T. Bailey, and J. K. Uhlmann, "Using exponential mixture models for suboptimal distributed data fusion," in *Proc. IEEE Nonlinear Stat. Signal Process. Workshop*, Cambridge, U.K., Sep. 2006, pp. 160–163.
[63] S. J. Julier and J. K. Uhlmann, "A non-divergent estimation algorithm in the presence of unknown correlations," in *Proc. Amer. Control Conf.*, Jun. 1997, PP. 2369–2373.
[64] M. Üney, S. Julier, D. Clark, and B. Ristić, "Monte carlo realisation of a distributed multi-object fusion algorithm," in *Proc. Sensor Signal Process. Defence (SSPD)*, Sep. 2010, pp.1–5.
[65] B. Wei, B. Nener, and W. Liu, "Tracking of space debris via CPHD and consensus," in *Proc. Int. Conf. Control, Automat. Inf. Sci. (ICCAIS)*, pp. 436–441, Oct. 2015.
[66] M. Morton and T. Roberts, "Joint space operations center (JSPOC) mission system (JMS)," DTIC Document, Vandenberg Air Force Base, CA, USA, Tech. Rep. JMS281, 2011.
[67] B. Wei, B. Nener, W. Liu, and L. Ma, "Centralized multi-sensor multi-target tracking with labeled random finite sets," in *Proc. Int. Conf. Control, Automat. Inf. Sci. (ICCAIS)*, Oct. 2016, pp. 82–87.
[68] K. Hill and B. Jones, "Turboprop version 4.0," *Colorado Center for Astrodynamics Res.*, 2009.
[69] S. J. Julier and J. K. Uhlmann, "New extension of the Kalman filter to nonlinear systems," *Proc. SPIE*, vol. 3086, pp. 182–193, Jul. 1997.
[70] C. R. McInnes, "Solar radiation pressure," in *Solar Sailing*. London, U.K.: Springer, 1999, pp. 32–55.
[71] A. Milani, A. M. Nobili, and P. Farinella, *Non-Gravitational Perturbations and Satellite Geodesy*. A. Milani, A. M. Nobili, P. Farinella, Eds. Bristol, U.K.: Adam Hilger Ltd., 1987.
[72] K. G. Murty, "An algorithm for ranking all the assignments in order of increasing cost," *Oper. Res.*, vol. 16, no. 3, pp. 682–687, May/Jun. 1968.
[73] S. Gehly, B. Jones, and P. Axelrad, "An AEGIS-CPHD filter to maintain custody of GEO space objects with limited tracking data," in *Proc. Adv. Maui Opt. Space Surveill. Technol. Conf.*, Sep. 2014, p. 25.
[74] G. Schwarz, "Estimating the dimension of a model," *Ann. Statist.*, vol. 6, no. 2, pp. 461–464, 1978.
[75] M. Beard, B. T. Vo, B.-N. Vo, and S. Arulampalam, "A partially uniform target birth model for Gaussian mixture PHD/CPHD filtering," *IEEE Trans. Aerosp. Electron. Syst.*, vol. 49, no. 4, pp. 2835–2844, Oct. 2013.
[76] F. Xiao and L. Wang, "State consensus for multi-agent systems with switching topologies and time-varying delays," *Int. J. Control*, vol. 79, no. 10, pp. 1277–1284, Feb. 2006.
[77] N. Chopra and M. W. Spong, "Output synchronization of nonlinear systems with relative degree one," in *Recent Advances in Learning and Control*. Springer, pp. 51–64, 2008.
[78] Z. Li, Z. Duan, G. Chen, and L. Huang, "Consensus of multiagent systems and synchronization of complex networks: A unified viewpoint," *IEEE Trans. Circuits Syst. I, Reg. Papers*, vol. 57, no. 1, pp. 213–224, Jan. 2010.
[79] D. Schuhmacher, B.-T. Vo, and B.-N. Vo, "A consistent metric for performance evaluation of multi-object filters," *IEEE Trans. Signal Process.*, vol. 56, no. 8, pp. 3447–3457, Aug. 2008.

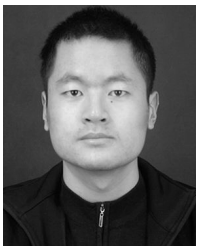

BAISHEN WEI received the B.E. and M.E. degrees from Harbin Engineering University, in 2010 and 2012, respectively, and the Ph.D. degree from The University of Western Australia, in 2017. He is currently a Lecturer with the School of Mechanical and Electric Engineering, Guangzhou University. His current research interests include multi-target tracking and multi-sensor fusion, space situational awareness, and cell tracking.

BRETT D. NENER received the B.E. and Ph.D. degrees from The University of Western Australia, in 1977 and 1987, respectively, and the M.E.Sc. degree from The University of Tokyo, in 1980. He has been a Visiting Professor with the U.S. Navy Space and Naval Warfare Center, San Diego, CA, USA, the University of California at Santa Barbara, and the Japanese National Institute of Information and Communications Technology (NICT). He is currently a Professor with the Department of Electrical, Electronic and Computer Engineering, The University of Western Australia, where he was the Head of the School, from 2008 to 2014. His current research interests include biosensors; III–N devices; modeling of atmospheric effects such as refraction, scintillation, and aerosol scattering; electro-optic systems; and infrared and UV photodetector devices and models.